An Autonomous Molecular Bioluminescent Reporter (AMBER) for voltage imaging in freely moving animals

Prasanna Srinivasan[1∞], Nicole M Griffin[1*], Pradeep Joshi[2*], Dhananjay Thakur[2*], Alex Nguyen-Le[1#], Sean McCotter[1, 4 #], Akshar Jain[1#], Mitra Saeidi[1#], Prajakta Kulkarni[1#], Jaclyn Eisdorfer[3], Joel Rothman[2], Craig Montell[2], Luke Theogarajan[1∞]

[1]Department of Electrical and Computer Engineering, Harold Frank Hall, University of California Santa Barbara, CA 93106
Center for Bioengineering, Institute for Collaborative Biotechnologies, University of California Santa Barbara, CA 93106

[2]Department of Molecular, Cellular and Developmental Biology and the Neuroscience Research Institute, University of California Santa Barbara, CA 93106

[3]Department of Bioengineering, Temple University, Philadelphia, PA 19122

[4]Senseeker Engineering, Goleta, CA 93117

[* #] Equal contribution
[∞]Corresponding authors: lusthe@ucsb.edu; prasri@ucsb.edu

1. Abstract

Genetically encoded reporters have greatly increased our understanding of biology, especially in neuroscience. While fluorescent reporters have been widely used, light delivery and phototoxicity have hindered their utility. Bioluminescence overcomes some of these challenges but requires the addition of an exogenous luciferin limiting its use. Using a modular approach we have engineered Autonomous Molecular BioluminEscent Reporter (AMBER), an indicator of membrane potential. Unlike other luciferase-luciferin bioluminescent systems AMBER encodes the genes to express both the luciferase and luciferin. AMBER is a voltage-gated luciferase coupling the functionalities of the Ciona voltage sensing domain (VSD) and bacterial luciferase, luxAB. When AMBER is co-expressed with the luciferin producing genes it reversibly switches the bioluminescent intensity as a function of membrane potential. Utilizing both biophysical and biochemical methods we show that unlike other voltage indicators AMBER modulates its enzymatic activity as a function of the membrane potential. AMBER shows a several fold increase in the luminescent (ΔL/L) output upon switching from off to on state when the cell is depolarized. *In vivo* expression of AMBER in *C. elegans* allowed detecting pharyngeal pumping action and mechanosensory neural activity from multiple worms simultaneously. Since we are able to report neural activity of multiple animals at the same time, we believe AMBER can be used in social behavior assays to elucidate the role of membrane potential underlying the behaviors.

2. Introduction

Genetically encoded molecular reporters have greatly improved our understanding of protein-protein interactions, gene expression and cellular signaling. Most reporters transduce the signal of interest into an optical readout via excitation of a fluorescent protein [1]. Application of molecular engineering to detect, record and modulate neural signatures is a major area underpinning neurotechnology initiatives. Over the last decade, there has been exponential growth in the development of optical neural probes. In particular, genetically encoded sensors are usually preferred due to their ability to precisely target cells of interest. A wide range of biomolecular sensors currently exists for detecting neural activity– calcium [2-4], voltage [3,5], potassium [6,7] and neurotransmitters [3]. While fluorescent reporters have been the mainstay, it suffers from tissue scattering, phototoxicity, photobleaching and autofluorescence affecting its long-term use [8]. Near-infrared indicators [4,9,10] and two-photon excitation [11,12] overcome some of these limitations, but the development of efficient indicators of neural activity remains an issue.

Intracellular calcium (Ca^{2+}) concentration and membrane potential are the two well-characterized proxies of neuronal activities. Several genetically encoded Ca^{2+} indicators (GECIs) [2-4, 13] were developed over the last two decades of which GCaMP variants [14] are the most widely used in the neuroscience community. However, the relationship between calcium signals and neuronal activity can vary among different neuronal types and may become completely uncoupled. For instance, besides diverse organelle dependent (endoplasmic reticulum and mitochondria) Ca^{2+} buffering, several Ca^{2+} binding proteins are differentially expressed at high levels in various parts of the brain [15]. Over expression of GECIs in these neurons can cause these Ca^{2+} responsive probes to contribute to Ca^{2+} buffering, thereby affecting the neurophysiological conditions [16]. Secondly, despite its high signal-to-noise ratio (SNR), GECIs cannot report subthreshold or hyperpolarizing events in neurons [17,18]. In contrast, fluorescent GEVIs allow recording both sub-threshold and threshold events from a few tens of neurons [19] simultaneously. Recently, neural spike were recorded from a large population of neurons (~ 100) for several minutes using a fluorescent hybrid GEVI [20] but requires a molecular complexation with a synthetic dye. Given the spike duration and the firing rates, there is a technical challenge in achieving a good SNR (> 5 as per Rose criterion [21]) at a frame rate of ~1kHz even with the best performing GEVI. Molecular reporters with a long shelf

life enable long-term recordings and this when coupled with rigorously controlled experimental condition will allow dissecting information processing in a large population of neurons.

Recently bioluminescence has garnered attention as an alternative to overcome some of the limitations of GEVIs and GECIs [22]. Bioluminescent imaging does not require any external illumination and light emission is achieved as a byproduct of a biochemical reaction – oxidation of a substrate (luciferin) catalyzed by an enzyme (luciferase). Commonly preferred light generating luciferase from firefly and marine organisms such as Aequoria, Renilla, Gaussia, Metridia, and Vargula [23-27] require exogenous addition of luciferin because biosynthetic pathways for in-situ luciferin production have not been elucidated yet. The inability of the luciferin in crossing the cell membrane makes delivery inefficient and precludes their use as a neural reporter, though some have been used for reporting slow Ca^{2+} signaling in neural networks [28-30]. Key advances have been made to improve the brightness of these bioluminescent probes using bioluminescent resonant energy transfer (BRET) [31] and directed evolution of fire-fly luciferase for a synthetic luciferin analogue [32]. LOTUS-V [33] was the first Luminescent Voltage Indicator (LuVI) created using an engineered deep-sea shrimp luciferase (Nluc) and Venus. LOTUS-V allows stable expression in mice *in vivo* [34] but the luciferin (furimazine) needs to be supplied exogenously.

The central drawback in most bioluminescent systems is the requirement of a luciferin, the light producing substrate. While the genes required for expressing different luciferases are known, the genes required for expressing luciferins have not been identified yet. There are two exceptions – the genes coding for the fungal luciferin, 3-hydroxyhispidin [35] and the bacterial luciferin, a molecular complex of fatty aldehyde and reduced flavin mononucleotide, $FMNH_2$ [36]. In a tour-de-force, Yampolsky et. al discovered a set of genes required for expressing both the fungal luciferase and luciferin [37]. However, the fungal bioluminescence system requires a total of seven genes assembled from multiple organisms and it can be challenging to express efficiently in eukaryotic systems. In contrast, the bacterial *lux* operon genes are encoded in a single polycistronic mRNA [38], and enables enhanced bioluminescence at a resolution of a single bacterium [39].

The *lux* operon, unlike other bioluminescent systems, consists of a series of six genes *(luxCDABE* and *frp*) synergistically combining to produce both the luciferase and a luciferin-generating secondary protein complex. The luciferin synthesizing protein complex recycles the products and intermediates of the light reaction endogenously using metabolic pathways [38]. *luxA* and *luxB* gene products form a 1:1 heterodimeric complex acting as the luciferase enzyme. The remaining *luxCDE* genes encode for a secondary 4:4:4 tetrameric trimer substrate processing complex that generates a long chain fatty aldehyde (myristyl aldehyde or tetradecanal, $C_{14}H_{28}O$), from fatty acids resulting from lipid biogenesis, to act as the primary substrate for the bioluminescent reaction (Figure 1). The other substrate, $FMNH_2$ and molecular oxygen (O_2) are metabolic products of host cell environment. Fortuitously, tetradecanal is not freely available in large quantities in eukaryotes [40], ensuring low background activation. There were concerns about apparent cytotoxic effects of aldehyde compounds in eukaryotes [41] but the concentration of tetradecanal synthesized using *lux* operon expression does not seem to attain the toxic dose affecting cell viability [40]. Recent work has also confirmed there is no cytotoxic effect when lux cassette is expressed in mammalian cells [42].

In this paper we describe a particular type of LuVI named AMBER (Autonomous Molecular BioluminEscent Reporter) for observing neural activity in freely moving animals. AMBER uses the functionalities of the ascidian *Ciona intestinalis* voltage sensing domain (Ci-VSD) [43],

bacterial luciferase, luxAB [40] (derived from P. *luminescens*), and a fluorescent moiety, YPet [44] fused to the C-terminus. We leveraged our probe design using the molecular architecture of a previously developed GEVI, VSFP2.1 [45]. The rationale behind this choice stems from the efficient coupling between conformational change of VSD and the positioning of Cerulean/Citrine FRET pairs at C-terminus of VSFP2.1. We critically assessed the functional equivalence of luxAB-YPET BRET pair for replacing Cerulean/Citrine FRET pair in VSFP2.1 using structure-function relationship of protein domains. Firstly, both YPet and Citrine share a similar beta-barrel structural arrangement and their exchange should not greatly influence the probe function. On the other hand, *P. luminescens* luxAB (pluxAB) structure is not yet solved although it shares a comparable protein sequence identity (89% *luxA* and 54% *luxB*) with V. *harveyi* luxAB (vluxAB) whose structure is known [46, 47]. vluxAB halo enzyme under low salt condition show discrete vluxA and vluxB domains with almost an identical $(\beta/\alpha)_8$ barrel structure [46]. Fusion of vluxA and vluxB domains with a polypeptide linker catalyze light reaction and it activity varies with linker length [48]. We therefore hypothesized that replacing FRET pair of VSFP2.1 with the compact luxAB/YPet BRET pair is a good starting point for subsequent structural optimizations. Surprisingly, we discovered a much richer enzymatic switching mechanism that provides an unprecedentedly large dynamic range in the optical readout (several fold increase in the fractional luminescence change ($\Delta L/L$)). We also increased the efficiency of the biophotonic emission by positioning a flavin reductase in the N-terminus of VSD and produced the luciferin in situ by co-expressing the luxCDE genes. Unlike other voltage probes reported to date AMBER undergoes a change in the enzymatic activity upon depolarization. The depolarization also resulted in some BRET, and the coupled mechanisms resulted in a 10X change in bioluminescence. We expressed the optimized first generation of AMBER in C. *elegans* pharyngeal muscles and mechanosensory neurons to demonstrate its in vivo use. AMBER allowed recording neural signatures of freely moving multiple animals in different directions simultaneously, which is not possible with stage feedback normally used in fluorescent imaging approaches.

3. Results:

3.1 Optimizing engineered AMBER Constructs: We postulated voltage sensing ability can be conferred to the *lux*-based LuVI by replacing the fluorescent FRET donor, Cerulean, of VSFP2.1 [45] with the mammalian codon optimized synthetic luciferase, enhanced luxAB [49] (henceforth called as 'eluxAB'. See section 1 in the Supporting Information, SI). The Citrine domain of VSFP2.1 was modified to YPet, the brightest variant of YFP whose absorption spectrum substantially overlap with a broad luxAB emission spectrum. Fused luxAB retains its enzymatic activity [48]; therefore, we created a fusion linker between eluxA and eluxB by mutating the conserved proline and glycine of a self-cleaving viral2A peptide to alanines [50]. Implementation of these modifications to the VSFP2.1 plasmid results in a plasmid coding for VSD-eluxAB-YPet protein. The remaining components of lux operon, lux*CDE-frp* was kept intact in the $pCMV_{lux}$ backbone allowing polycistronic co-expression of luxCDE-FRP along with the membrane-targeted VSD-eluxAB-YPet. Previous reports on BRET pairs show the position of the acceptor can influence the brightness of the probe. We therefore swapped the position of eluxAB and YPet (designated VSD-YPet-eluxAB) to test the effect of the acceptor position on the performance of our probe. Plasmids encoding different engineered protein constructs were expressed in HEK293 cells (See section 2 in the SI). Bioluminescent images captured in a dark room using a custom-built microscope mounted with an EMCCD camera (See Section 3 in the SI) were processed using the ImageJ software (See Section 10 in the SI). Initial testing by addition of 50mM KCl to the media showed VSD-eluxAB-YPet performed better than VSD-YPet-eluxAB. Secondly, Flavin mononucleotide (FMN) is known to be the rate limiting substrate in bacterial bioluminescence reaction [51]. Furthermore, there are evidences for the direct transfer

of reduced flavin to luxAB from flavin reductase phosphate (FRP), Moreover, fusion constructs linking FRP and luxAB have significantly higher quantum yields [52,53]. We therefore hypothesized that by localizing FRP close to eluxAB in the membrane-targeted construct, the light intensity can further be increased. The FRP domain was therefore introduced at the N-termini of both VSD-YPet-eluxAB and VSD-eluxAB-YPet constructs resulting in probes designated as FRP-VSD-YPet-eluxAB and FRP-VSD-eluxAB-YPet respectively (See section 1 in the SI). Surprisingly FRP-VSD-YPet-eluxAB performed the poorest of the constructs tested. However, as expected FRP-VSD-eluxAB-YPet performed the best, validating our hypothesis. Results from all the engineered constructs before and after KCl addition are shown in Figure 2a. The signal-to-noise ratio (SNR) of various constructs (Figure 2b) obtained using KCl depolarization indicates that the FRP-VSD-eluxAB-YPet construct performed the best among the engineered constructs tested (Figure S2). Both untransfected HEK293 cells (Figure S1) and endogenous substrates on its own (Figure S3) resulted in a very low background signal – about 10 times smaller to the maximum achieved even after integrating for 30s.

3.2 Plate reader assay: A large increase in the bioluminescent signal after KCl challenge precludes the dominant mode from being a resonant energy transfer mechanism and so we performed a more quantized analysis using a plate reader. Luminescence spectrum of HEK293 cells expressing the bright construct was collected before and after KCl addition (See Section 4 in the SI). Figure 2c provides direct evidence for an increase in both the luxAB donor peak at 490nm and the YPet acceptor peak at 530nm upon KCl depolarization, with a relatively lower activity before the addition of KCl.

3.3 Dark Mutant: Additional evidence to confirm the enzymatic switching upon depolarization was obtained by mutating the YPet chromophore residues (G65T and G67A of the chromophore residues [54]) of FRP-VSD-eluxAB-YPet (See section 1 in the SI). This mutational change (termed 'dark mutant'), greatly diminish the possibility of BRET, if any. Bioluminescent imaging of HEK293 cells expressing the dark mutant showed increase in the intensity upon depolarization using KCl (Figure 3). Plate reader experiments using the dark mutant also showed an increase in the spectral intensity at 490nm upon depolarization suggesting modulation of the enzymatic activity of the probe as the dominant mode of the light emission (See Section 4 and Figure S5 in the SI).

3.4 NADH Assay: Tracking NADH production provides an indirect evidence for eluxAB enzymatic activity because NADH production increase with the drop in molecular O_2 concentration. NADH is utilized both for regenerating $FMNH_2$ from FMN catalyzed by FRP and for the fatty aldehyde synthesis from fatty acid via luxCDE complex. While the reduced form (NADH) is fluorescent, the oxidized form (NAD+) is non-fluorescent. We monitored the endogenous NADH fluorescence before and after KCl addition, which shows an increase in the NADH signal after KCl addition (See Sections 3, 10 and Figure S6 in the SI). We confirm the causal link between the enzymatic switching of the bioluminescent probe and the O_2 consumption by the light reaction i.e. increase in the NADH fluorescence. While the steady-state NADH fluorescence before KCl addition is not large enough to be detected, a step increase after KCl addition invariably points to the drop in O_2 concentration. Cytosolic NADH is produced at detectable levels within a few seconds after O_2 consumption in the light reaction and similar such observations were reported in earlier work [55]. This result also suggests that the steady-state aldehyde concentration in cells is sufficient to carry out the light reaction for a long duration (at least for a few tens of minutes) because NADH production rate due to O_2 drop is faster than rate of NADH consumption for aldehyde synthesis. Our argument here on the NADH rise is only to establish the causal link between the light reaction and the drop in free O_2 concentration. We rule out the cell viability concerns due to hypoxia in this context because

prolonged unilateral rise in membrane potential after KCl addition does not represent physiologically controlled cellular depolarization states.

3.5 Voltage switching characterization: We performed electrophysiology experiments to determine the voltage dependent characteristics of the probe. We transiently co-expressed FRP-VSD-eluxAB-YPet and luxCDE in HEK293 cells to record single cell bioluminescence under voltage clamp. Results from the patch clamp experiment are shown in Figure 4a (See section 5 in the SI). The switching threshold, $V_{1/2}$ is ~ –30mV is within the physiological range of neuronal action potential similar to other GEVIs reported in literature [56-58]. A corollary to this result is depolarization of HEK293 cells co-expressing the bright construct (with luxCDE) and VSD-YPet-eluxAB (with luxCDE-FRP) separately by titrating with incremental amounts of KCl (Figure 4b). The $V_{1/2}$ deduced applying Nernstian relation to the KCl titration data agrees closely with the value obtained via patch clamp recordings. Interestingly, $V_{1/2}$ is more positive compared to that of VSFP2.1 ($V_{1/2}$ is ~ –70 mV) from which it was derived and agrees closely with the switching threshold of VSFP2.3, indicating the interaction between the eluxAB and the VSD domain. Additionally, $V_{1/2}$ shifts towards positive for FRP-VSD-eluxAB-YPet compared to VSD-YPet-eluxAB. We do not know if the BRET pair interacts with the VSD domain and its rearrangement caused the voltage shift. Earlier work showed evidences for the interaction between fluorescent protein and the VSD domain but the mechanism of fluorescence modulation by VSD is still not fully understood [55]. We speculate the interaction between the YPET and the VSD domains could be a possible reason for the observed shift.

3.6 Chemogenetic activation: Since an increase in extracellular K^+ affects many cellular signaling processes, we wanted to independently verify if enzymatic switching could be achieved using a different chemical activator under physiological condition. We co-expressed rat TRPV1 (rTRPV1) with the bright probe construct (and its substrate luxCDE) in HEK293 cells and stimulated using Capsaicin. TRPV1 has a large single channel conductance and Capsaicin is a known to activate TRPV1 allowing a large ionic current causing cellular depolarization [59]. Bioluminescence experiments performed under these conditions also exhibited change in bioluminescence signals when subjected to the chemical stimulus (See section 3 and Figure S4 in the SI)

3.7 In vivo Activity of AMBER: We created *C. elegans* transgenic lines to demonstrate AMBER function invivo. Our choice of the model organism is driven by the optically transparent properties of their tissues and the slow kinetics of muscle and neuronal voltage signals (about few seconds). We subcloned both the probe and substrate plasmids into *C.elegans* expression vectors that target pharyngeal muscles and mechanosensory neural circuit using the Myosin-2 heavy chain gene, *myo-2* promotor [60] and the β-tubulin gene, *mec-7* promotor [61,62], respectively. The later promotor drives expression in several mechanosensory touch neurons (ALMR, ALML, AVM, PLMR, PLML, PVM) and the anterior nerve ring (See SI for *mec-7* promoter driven eGFP expression in *C.elegans*). We used a custom-built imaging set up to record bioluminescent signal, while simultaneously tracking the positions of the animal (See SI). Signals from the touch neurons did not show any activity when the worm was moving unilaterally in the forward direction but showed bursts of activity while making spatially localized movements and frequent reversals (See supplementary movie SM1 and Figure 5a) or during collisions (Figure5b). Earlier work reported mechanosensory touch neurons respond to differential force, but not to the exertion of a constant force [63, 64]. The activity of the touch neurons during collision between animals is perhaps due to transient differential forces due to momentum conservation under collision. The underlying mechanics in other cases (frequent reversals and localized movements) could not be teased out although it is known that such

motions on the agar bed help the animals to detect bacteria on the plate [65]. A huge advantage of AMBER is the ability to simultaneously record the activity of a neural circuit from multiple worms moving in different directions within the field of view, which is not possible using fluorescence (Figure 5c and Supplementary Movie SM2).

In contrast, rhythmic voltage activity of the pharyngeal muscles correlates well with the muscle movement, which agrees closely with the results, obtained using fluorescent GEVI [66]. We plotted the voltage activity and the muscle movement obtained from the brightfield images (Figures 6a-b and Supplementary Movie SM3). Additionally, we also showed filtered signal of the voltage activity recorded by the AMBER. A close correspondence between the filtered trace and the muscle movement confirms the validity of the AMBER function (See SI for additional traces). The reflection of the muscle movement in the voltage trace provides clear evidence to the utility of the probe in assaying voltage activity *in vivo*.

4. **Discussion**: We reported the performance of a first generation voltage sensitive bioluminescent probe (AMBER) that uses a Ciona VSD and a synthetic enhanced bacterial luciferase, eluxAB. The biochemistry of the light generation can be summarized by the following set of reactions.

$$\begin{aligned} &FMNH_2 + RCHO + O_2 \rightarrow FMN + RCOOH + H_2O + h\nu_{490nm} \\ &FMN + NAD(P)H + H^+ \rightarrow FMNH_2 + NAD(P)^+ \qquad (1) \\ &RCOOH + ATP + NAD(P)H + H^+ \rightarrow RCHO + AMP + PPi + NAD(P)^+ + H_2O \end{aligned}$$

As mentioned earlier the lux system is autonomous and enables expression of both the probe and substrate, circumventing the major drawback of other bioluminescent systems. The fusion between the VSD and luxAB results in a membrane protein capable of modulating its luminescence output. We optimized the light emission from the probe applying rational molecular engineering approach. Modifications included mutating luxAB to a brighter eLuxAB, modifying the viral 2A peptide to enable a fusion linker, relative placement of the luciferase and YPet and the fusion of the FRP reductase enzyme at the N-terminus to achieve direct transfer of $FMNH_2$ reducing the loss to the dark pathway by $FMNH_2$ auto-oxidation. For all experiments we co-expressed the luxCDE complex necessary to generate the fatty acid aldehyde, which serves as the luciferin. While the presence of the fluorescent protein enables BRET, it does not appear to be the dominant mechanism. Instead our studies show that an increase in the luxAB catalytic activity as the primary contributor of the light emission though there is evidence of some BRET.

While we were unable to fully elucidate the switching mechanism we performed multiple experiments to rule out several alternate mechanisms. Direct modulation of fluorescence is known to occur in GEVIs that are fused directly to the C-terminus of Ci-VSD. However, we ruled this mechanism, by designing a construct with eluxAB fused to the C-terminus of VSD. Though the construct showed some weak signals (see SI) it did not show a large change in the light emission as observed in the FRP-VSD-eluxAB-YPet. Dimerization of the acceptor fluorescent protein causes voltage dependent FRET in fluorescent GEVIs [67]. We ruled this mechanism using a dark mutant of YPet that showed voltage dependent bioluminescent signal but no acceptor resonance energy transfer. However, one cannot rule out the possibility of YPet structurally modulating the coupling between eluxA and eluxB domains. To rule this out we used the construct that has both the YPet and luxAB switched (FRP-VSD-YPet-eluxAB). Interestingly, this construct was the poorest performing in the constructs we tested. If the movement of the VSD S4 domain had caused a non-optimal coupling between eluxA and eluxB aided by the presence of YPet, this construct should increase the effect since the YPet is closer to VSD then eluxAB. However, one could argue the position of YPET could have prevented dimerization and

hence the modulation. In that case, the probe should constantly be emitting light because the YPet is undimerized and the eluxAB is further removed from the VSD and this is not observed in experiments. The availability of reduced FMN ($FMNH_2$) necessary for light production (see reactions 1) is a limiting substrate and when coupled to the VSD enables luminescence modulation. However, we also excluded this mechanism as well. We generated constructs with/without FRP, the reductase enzyme, which converts FMN to $FMNH_2$. Though the brightest construct was the one with FRP on the N-terminus (with the optimal positioning of eluxAB and YPet), when compared to their counterparts with YPet and eluxAB in non-optimal positions, the constructs without FRP showed higher modulation eliminating the validity of this proposal. Lastly, the movement of the VSD could modulate the accessibility of the substrate to eluxAB. This can be partially eliminated by looking at the results from the construct with the positions of eluxAB and YPET switched. The eluxAB positioned close to the C-terminus should allow maximum accessibility to the substrate, which should produce a brighter signal. Furthermore, there should be a sustained background bioluminescence, which we did not observe in our experiments.

We suggest that one plausible mechanism accounting for the voltage dependent activity could be the structural arrangement of the optimal construct (FRP-VSD-eluxAB-YPet). This construct prevents the substrate access to eluxAB before depolarization and adopts an open confirmation when the voltage changes.

One experiment that is conspicuously absent is the kinetics of switching. Currently our experimental setup does not allow us to quantify the switching kinetics. However, some general trends can be observed based on the range of exposure times considered in our experiments. In most experiments the integration time was 1 second and we have been able to observe *in vivo* signals with a 500 msecs integration time at high expression levels of the probe. This can be easily seen in the experiments done on the worm, C. elegans. Expression in the pharyngeal muscles allow us to observe voltage signal changes with a 500 msec snapshot and enable correlation between muscle movement and the voltage signals (Figure 7).

While many improvements can be made to the probe, we have shown for the first time the ability to modulate the enzymatic activity of the eluxAB by varying the membrane potential to realize a voltage gated luciferase. We believe this can find broad applicability in voltage imaging using bioluminescence.

5. Conclusions:

We engineered an autonomous voltage sensitive bioluminescent reporter based on the bacterial luciferase system. The ability to genetically encode the luciferase and the luciferin overcomes many challenges involved in firefly and the deep-sea shrimp bioluminescent systems. By careful engineering we optimized the probe construct to produce the brightest signal upon depolarization. AMBER exhibits a voltage dependent enzymatic switching not observed in other similar systems (e.g. LOTUS-V). We successfully expressed and demonstrated the AMBER function both invitro (HEK293 cells) and *in vivo* (C. *elegans*). We report the activities of mechanosensory neural circuit and the pharyngeal muscle pumping from multiple animals using our probe. We believe this will greatly enhance the ability to track animal behaviors, while simultaneously monitoring the activities of neurons.

6. Acknowledgements

This work was partially funded by the Otis Williams Fellowship, the NSF neuronex and the ICB at UCSB. The authors are grateful to Prof. Sumita Pennathur for generously lending us the EMCCD camera, Prof. Spencer Smith for help with patch clamp and Prof. Nathan Shaner for insightful discussions.

7. References

1. Mehta, S. & Zhang, J. Reporting from the Field: Genetically encoded fluorescent reporters uncover signaling dynamics in living biological systems. *Annu Rev Biochem.* **80**, 375-401 (2011)
2. Tian, L., Andrew Hires, S., & Looger, L. L. Imaging neuronal activity with genetically encoded calcium indicators. *Cold Spring Harb protoc.* doi:10.1101/pdb.top069609 (2012)
3. Lin, M. Z., & Schnitzer, M. J. Genetically encoded indicators of neuronal activity. *Nat. Neurosci.* **19**, 1142-1153 (2016)
4. Qian, Y. et al. A genetically encoded near-infrared fluorescent calcium indicator. *Nat. Methods*, **16**, 171-174 (2019).
5. Xu, Y., Zou, P. & Cohen, A. E. Voltage imaging with genetically encoded indicators. *Curr. Opin. Chem. Biol*. **39**, 1-10 (2017).
6. Bischof, H. et al., Novel genetically encoded fluorescent probes enable real-time detection of potassium in vitro and in vivo. *Nat. Comm.* **8**, 1422 (2017).
7. Shen, Y. et al. Genetically encoded fluorescent indicators for imaging intracellular potassium ion concentration. *Commun. Biol.* **2**, 18 (2019).
8. Yang, H. H. & St-Pierre, F. Genetically encoded voltage indicators: Opportunities and Challenges. *J. Neurosci.* **36**, 9977-9989 (2016).
9. Abdelfattah, A. S., et al. A bright and fast red fluorescent protein voltage indicators that reports neuronal activity in organotypic brain slices. *J. Neurosci.* **36**, 2458-2472 (2016).
10. Monakhov, M. V. et al. Bright near-infrared genetically encoded voltage indicator for all-optical electrophysiology. Preprint at https://www.biorxiv.org/content/10.1101/536359v1 (2019)
11. Yang, W. & Yuste, R. Invivo imaging of neural activity, *Nat. Methods*. **14**, 349-359 (2017).
12. Stirman, J. N. et al. Wide field-of-view, multi-region two-photon imaging of neuronal activity in the mammalian brain. *Nat. Biotechnol.* **34**, 857-862 (2016)
13. Fosque, B. F. et al. Labeling of active neural circuits in vivo with designed calcium integrators. *Science*. **347**, 755-760 (2015).
14. Zhao, Y. et al. An expanded palette of genetically encoded Ca^{2+} indicators. *Science*. **333**, 1888-1891 (2011).
15. Burgoyne, R. D. Neuronal Calcium sensor proteins: Generating diversity in neuronal Ca^{2+} signaling. *Nat. Neurosci*. **8**, 182-193 (2007).
16. Grienberger, C. & Konnerth, A. Imaging calcium in neurons. *Neuron*. **73**, 862-885 (2012)
17. Knöpfel, T. Genetically encoded optical indicators for the analysis of neuronal circuits. *Nat. Rev Neurosci*. **13**, 687–700 (2012).
18. Antic, S. D., Empson, R. M. & Knöpfel, T. Voltage imaging to understand connections and functions of neuronal circuits. *J. Neurophysiol*. **116**, 135–152 (2016).
19. Piatkevich, K. D. et al. Population imaging of neural activity in awake behaving mice. *Nature*. **574**, 413-417 (2019).
20. Abdelfattah, A. S. et al., Bright and photostable chemigenetic indicators for extended invivo voltage imaging. *Science*. **365**, 699-704 (2019).
21. Rose, A. *Vision: Human and Electronic* (Springer, 2013).
22. Bando, Y., Sakamoto, M., Kim, S., Ayzenshtat, I. & Yuste, R. Comparative evaluation of genetically encoded voltage indicators. *Cell Reports*. **26**, 802-813 (2019)
23. Lorenz, W. W., McCann, R. O., Longiaru, M. & Cormier, M. J. Isolation and expression of a cDNA encoding renilla reniformis luciferase. *Proc. Natl Acad. Sci. USA* **88**, 4438–4442 (1991).
24. Markova, S. V., Golz, S., Frank, A. A., Kalthof, B. & Vysotski, E., S. Cloning and expression of cDNA for a luciferase from the marine copepod Metridia *longa*, a novel secreted bioluminescent reporter enzyme. *J. Biol. Chem.* **279**, 3212–3217 (2004).

25. Thompson, E. M., Nagata, S. & Tsuji, F. I. Cloning and expression of cDNA for the luciferase from the marine ostracod Vargula *hilgendorfii*. *Proc. Natl Acad. Sci. USA* **86**, 6567--6571 (1989).
26. Verhaegen, M. & Christopoulos, T. K. Recombinant Gaussia luciferase. Overexpression, purification, and analytical application of a bioluminescent reporter for DNA hybridization. *Anal. Chem.* **74**, 4378-4385 (2002).
27. Wood, K. V., Lam, Y. A. & McElroy, W. D. Introduction to beetle luciferases and their applications. *J. Biolumin. Chemilumin.* **4**, 289-301 (1989).
28. Drobac, E., Tricoire, L., Chaffotte, A., Guiot, E. & Lambolez, B. Calcium imaging in single neurons from brain slices using bioluminescent reporters. *J. Neuro. Res*. **88**, 695–711 (2010).
29. Martin, J., Rogers, K. L., Chagneau, C. & Brûlet, P. Invivo bioluminescence imaging of Ca^{2+} signaling in the brain of drosophila. *PLoS ONE*. **2**, e275 (2007).
30. Rogers, K. L. et al. Non-invasive invivo imaging of calcium signaling in mice. *PLoS ONE*. 2, e974 (2007).
31. Saito, K. et al. Luminescent proteins for high speed single-cell and whole-body imaging. *Nat. Commun.* **3**, 1262 (2012).
32. Iwano, S. et al. Single cell bioluminescence imaging of deep tissue in freely moving animals. *Science*, **359**, 935-939 (2018).
33. Inagaki, S. et al. Genetically encode bioluminescent voltage indicator, *Sci. Rep*. **7**, 42398 (2017).
34. Inagaki, S. et al. Imaging local brain activity of multiple freely moving mice sharing the same environment, *Sci. Rep*. **9**, 7460 (2019)
35. Kaskova, Z. M. et al. Mechanism and color modulation of fungal bioluminescence. *Sci. Adv.* **3**, e1602847 (2017)
36. Brodl, E., Winkler, A. & Macheroux, P. Molecular mechanisms of bacterial bioluminescence. *Comput. Struct. Biotechnol. J.* **16**, 551-564 (2018).
37. Kotlobay, A. A. et al. Genetically encodable bioluminescent system from fungi. *Proc. Natl Acad. Sci. USA* **115**, 12728–12732 (2018).
38. Shieh, Y. W. et al. Operon structure and cotranslational subunit association direct protein assembly in bacteria, *Science*, **350**, 678-80 (2015)
39. Gregor, C. et al. Strongly enhanced bacterial bioluminescence with the ilux operon for single-cell imaging. *Proc. Natl Acad. Sci. USA*. **115**, 962-967 (2018)
40. Close, D. M. et al. Autonomous bioluminescent expression of the bacterial luciferase gene cassette (*lux*) in a mammalian cell line. *PLoS ONE*, **5**, e12441 (2010).
41. Hollis, R. P. et al. Toxicity of the bacterial luciferase substrate,n-decyl aldehyde, to *Saccharomyces cerevisiae* and *Caenorhabditis elegans*. *FEBS lett*. **506**, 140–142 (2001).
42. Gregor, C. et al. Autonomous bioluminescence imaging of single mammalian cells with the bacterial bioluminescence system. Preprint at https://www.biorxiv.org/content/10.1101/798108v1 (2019)
43. Li, Q. et al. Structural mechanism of voltage-dependent gating in an isolated voltage-sensing domain. *Nat. Struct. Mol. Biol*. **21**, 244-252 (2014)
44. Nguyen A. W. & Daugherty, P. S. Evolutionary optimization of fluorescent proteins for intracellular FRET. *Nat. biotech*. **23**, 355–360 (2005).
45. Dimitrov, D. et al. Engineering and characterization of an enhanced fluorescent protein voltage sensor, *PLoS ONE*. **2**, e440 (2007).
46. Fisher, A. J. et al. Three-dimensional structure of bacterial luciferase from Vibrio *harveyi* at 2.4A^{o} resolution. *Biochemistry*. **34**, 6581-6586 (1995)
47. Baldwin, T.O. et al. Structure of bacterial luciferase. *Curr. Opin. Struct. Biol.* **5**, 798-809 (1995).
48. Olsson, O. et al. Engineering of monomeric bacterial luciferases by fusion of *luxA* and *luxB* genes in Vibrio *harveyi*. *Gene*. **81**, 335-347 (1989).
49. Cui, B. et al. Engineering an enhanced, thermostable, monomeric bacterial luciferase gene as a reporter in plant protoplasts. *PLoS ONE*. **9**, e107885 (2014).
50. Szymczak, A. L. et al. Correction of multi-gene deficiency invivo using a single 'self-cleaving' 2A peptide-based retroviral vector. *Nat. Biotech*. **22**, 589–594 (2004).
51. Lei, B. & Tu, S. Mechanism of reduced flavin transfer from Vibrio *harveyi* NAD(P)H-FMN oxidoreductase to luciferase. *Biochemistry*. **37**,14623--14629 (1998).
52. Tu, S. Activity coupling and complex formation between bacterial luciferase and flavin reductases. *Photochem. Photobiol. Sci.* **7**, 183–188 (2008).
53. Jawanda, N., Ahmed, K. & Tu, S. Vibrio *harveyi* Flavin reductase-luciferase fusion protein mimics a single-component bifunctional monooxygenase. *Biochemistry*. **47**, 368-377 (2008).

54. Kutrowska, B. W. et al. Folding and unfolding of a non-fluorecent mutant of green fluorescent protein. *J. Phys Condens Matter.* **18**, 285223 (2007)
55. Schaefer, P. M., Kalinina, S., Rueck, A., von Arnim, C. A. F. & von Einem, B. NADH Autoflluorescence – A marker on its way to boost bioenergetic research. *Cytometry A*. **95A**, 34-46 (2019).
56. Sung, U. et al. Developing fast fluorescent protein voltage sensors by optimizing FRET interactions. *PLoS ONE*. **10**, e0141585 (2015)
57. Akemann, W. et al. Effect of voltage sensitive fluorescent proteins on neuronal excitability. *Biophys. J.* **96**, 3959-3976 (2009)
58. Jin, L., Han, Z., Platisa, J., Wooltorton, J. R., Cohen, L. B. & Pieribone, V. A. Single action potentials and subthreshold electrical events imaged in neurons with a novel fluorescent protein voltage probe. *Neuron*. **75**, 779-785 (2012)
59. Cao, E., Cordero-Morales, J. F., Liu, B., Qin, F. & Julius, D. TRPV1 channels are intrinsically heat sensitive and negatively regulated by phosphoinositide lipids, *Neuron*. **77**, 667-679 (2013).
60. Okkema, P. G., Harrison, W. W., Plunger, V., Aryana, A. & Fire, A. Sequence requirements for myosin gene expression and regulation in Caenohabditis elegans. *Genetics.* **135**, 385-404 (1993)
61. Hamelin, M., Scott, I. M., Way, J. C. & Culotti J. G. The mec-7 beta-tubulin gene of Caenorhabditis elegans is expressed primarily in the touch receptor neurons. *EMBO J.* **11**, 2885-93 (1992)
62. Zhang, Y. et al. Identification of genes expressed in C. elegans touch receptor neurons. *Nature*. 418, 331-335 (2002)
63. Goodman, M. B. Deconstructing C.elegans sensory mechanotransduction. *Science.* **306**, 427-428 (2004).
64. Krieg, M., Dunn, A. & Goodman, M. B. Mechanical systems biology of C.elegans touch sensation. *Bioessays*. **37**, 335-344 (2015)
65. Goodman, M. B. *Mechanosensation* (*WormBook*, ed. The *C. elegans* Research Community, WormBook, 2006)
66. Hashemi, N. A. et al. Rhodopsin-based voltage imaging tools for use in muscles and neurons of Caenorhabditis *elegans*. *Proc. Natl Acad. Sci. USA* **116**, 17051-60 (2019)
67. Yi, B., Kang, B. E., Lee, S., Braubach, S. & Baker, B. J. A dimeric fluorescent protein yields a bright, red-shifted GEVI capable of population signals in brain slice. *Sci. Rep.,* **8**, 15199 (2018)

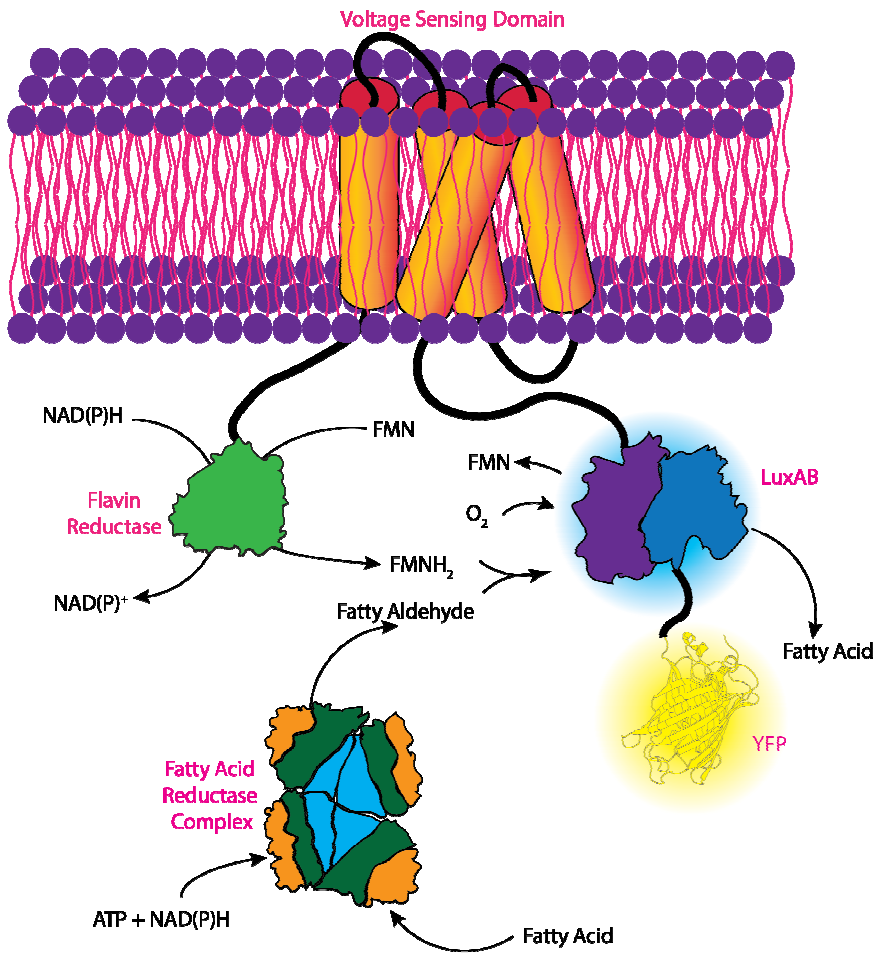

Figure 1: Schematic representation illustrating the molecular architecture of AMBER. AMBER is based on a membrane bound *Ciona* voltage-sensing domain (Ci-VSD) whose N and C termini are fused to Flavin reductase phosphate (FRP) and a BRET pair based on a bright bacterial luciferase bioluminescent donor (eluxAB) and a yellow fluorescent protein acceptor (YPET). An increase in membrane potential increases the probability of photon emission (λ_{max} ~ 490nm) by the luciferase which catalyses the reaction between a reduced flavin ($FMNH_2$), fatty aldehyde (synthesized by the fatty acid reductase complex) and molecular oxygen. The positioning of the Flavin reductase phosphate in the N-terminus reduces the auto oxidation of the reduced flavin by enabling direct shuttling between the luciferase and the flavin reductase.

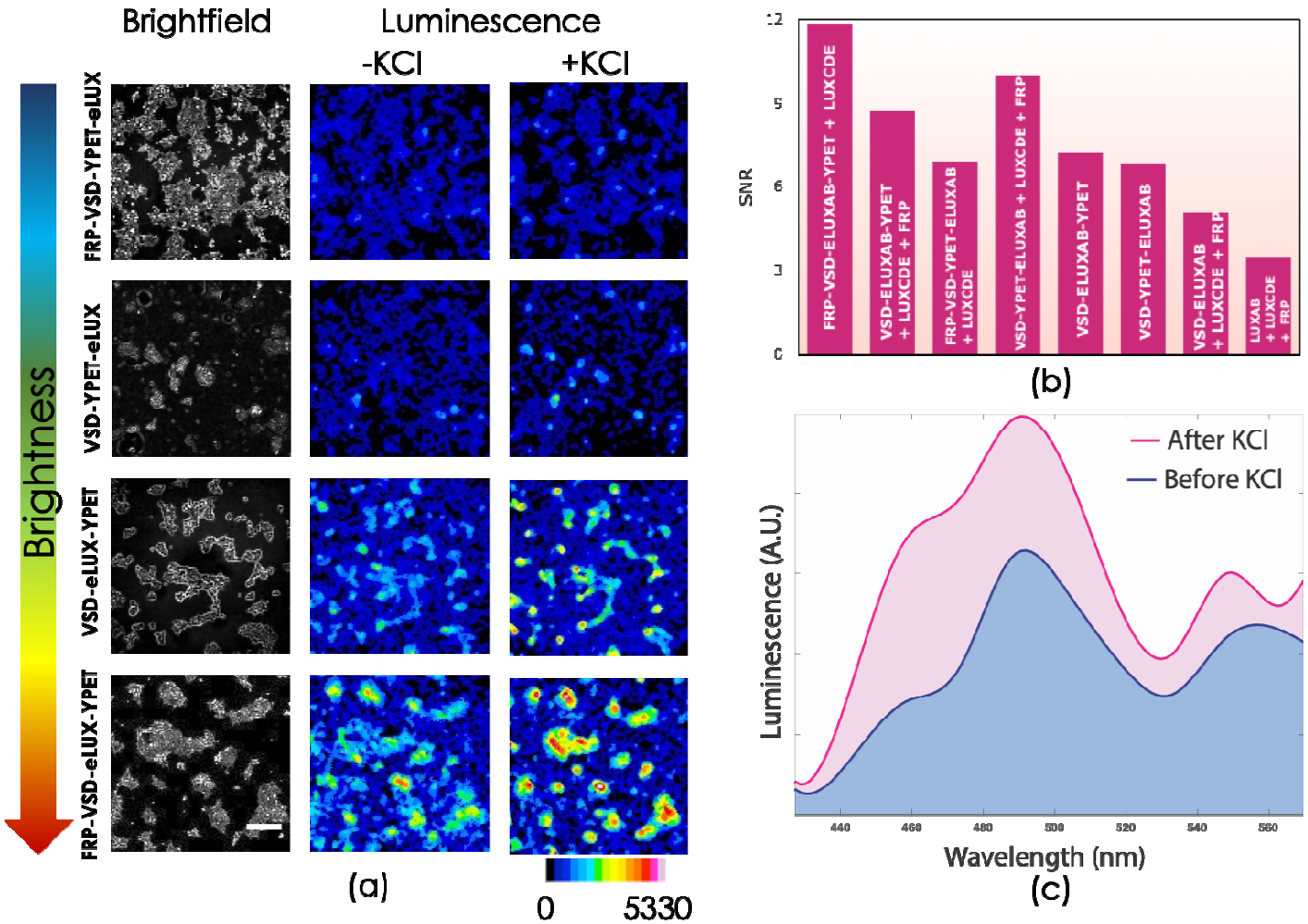

Figure 2: (a) Invitro bioluminescent performance before and after KCl challenge of various engineered protein constructs expressed in HEK cells. FRP-VSD-eluxAB-YPet delivered the best performance ($(\Delta L/L)_{max}$ ~ 28; $(\Delta L/L)_{avg}$ ~ 0.72; Average information transfer ~ 0.85 from more than n=80 cells). (b) Signal-to-noise ratio of various engineered constructs. Performance of majority of the constructs meet Rose criterion (SNR > 5) suggesting the signal is sufficiently higher than the background noise. (c) Emission spectra of HEK cells expressing the bright construct before and after KCl challenge. Photon counts for each spectral wavelength show the mean counts obtained from n=8 trials. The scale bar of the micrograph corresponds to 200µm

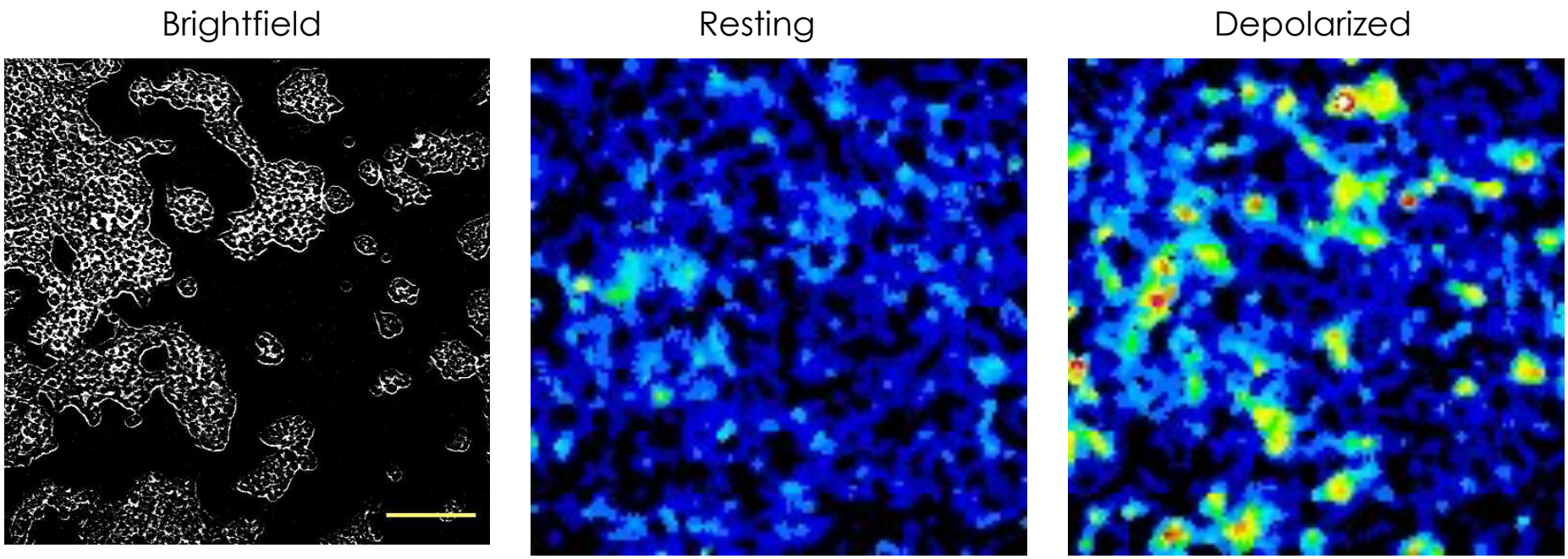

Figure 3: Biophotonic emission from the dark mutant probe expressed in HEK cells before and after KCl challenge. The data suggests the physical interaction between Ypet and eluxAB domains is the primary driver for the modulation of activity. BRET seems to play only a minor role in the transduction of the membrane potential into photon count. The scale bar corresponds to 200μm.

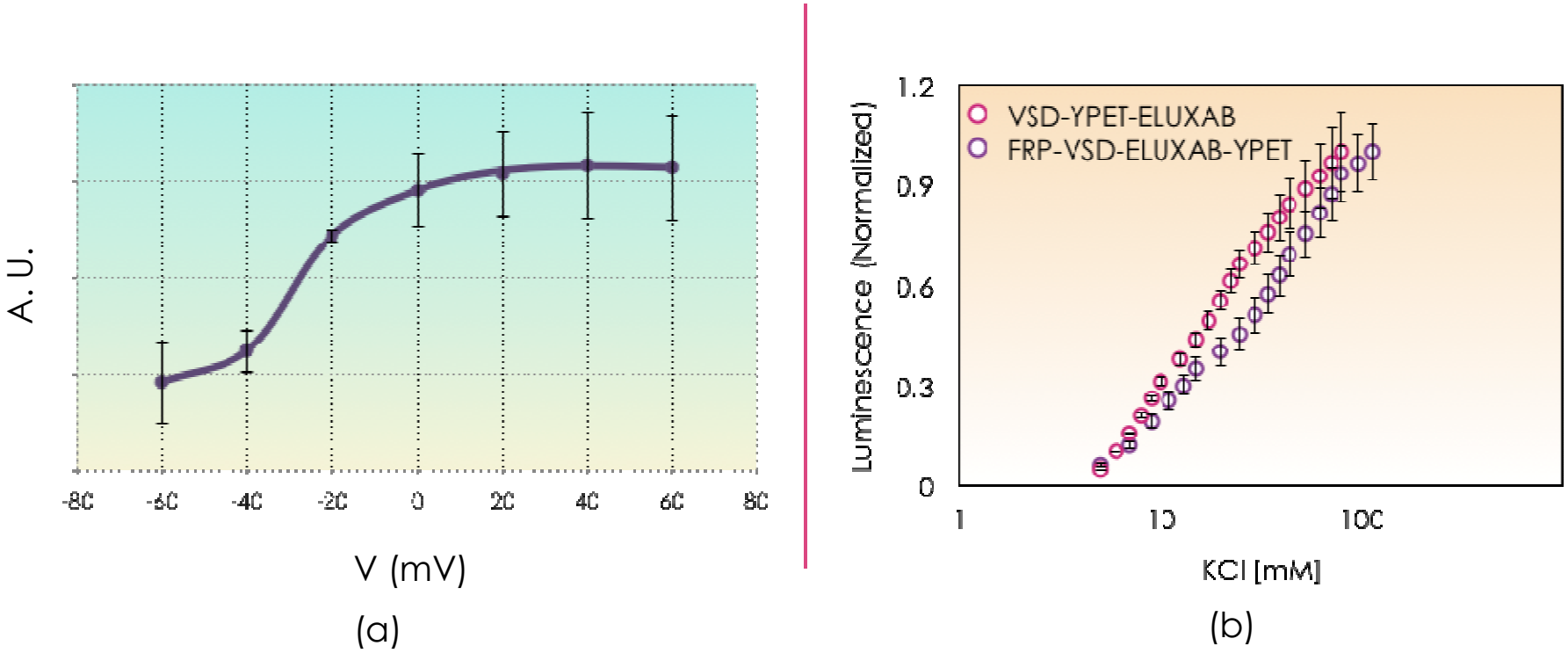

Figure 4: (a) Representative whole cell voltage clamp recording from a HEK293 cell expressing AMBER and its substrate. Paired measurements (n=6 repeats) were taken by varying the membrane potential between –60mV and 60mV in increments of 20mV. The intensity of the light emitted under electrical stimulation follows the classical Boltzmann distribution with $V_{1/2}$ ~ –30mV. (b) Normalized bioluminescent response of the top two high performing constructs under KCl titration. The semi-log plot suggests an order of magnitude change in the extracellular KCl concentration is necessary to achieve the maximum intensity for the chosen constructs.

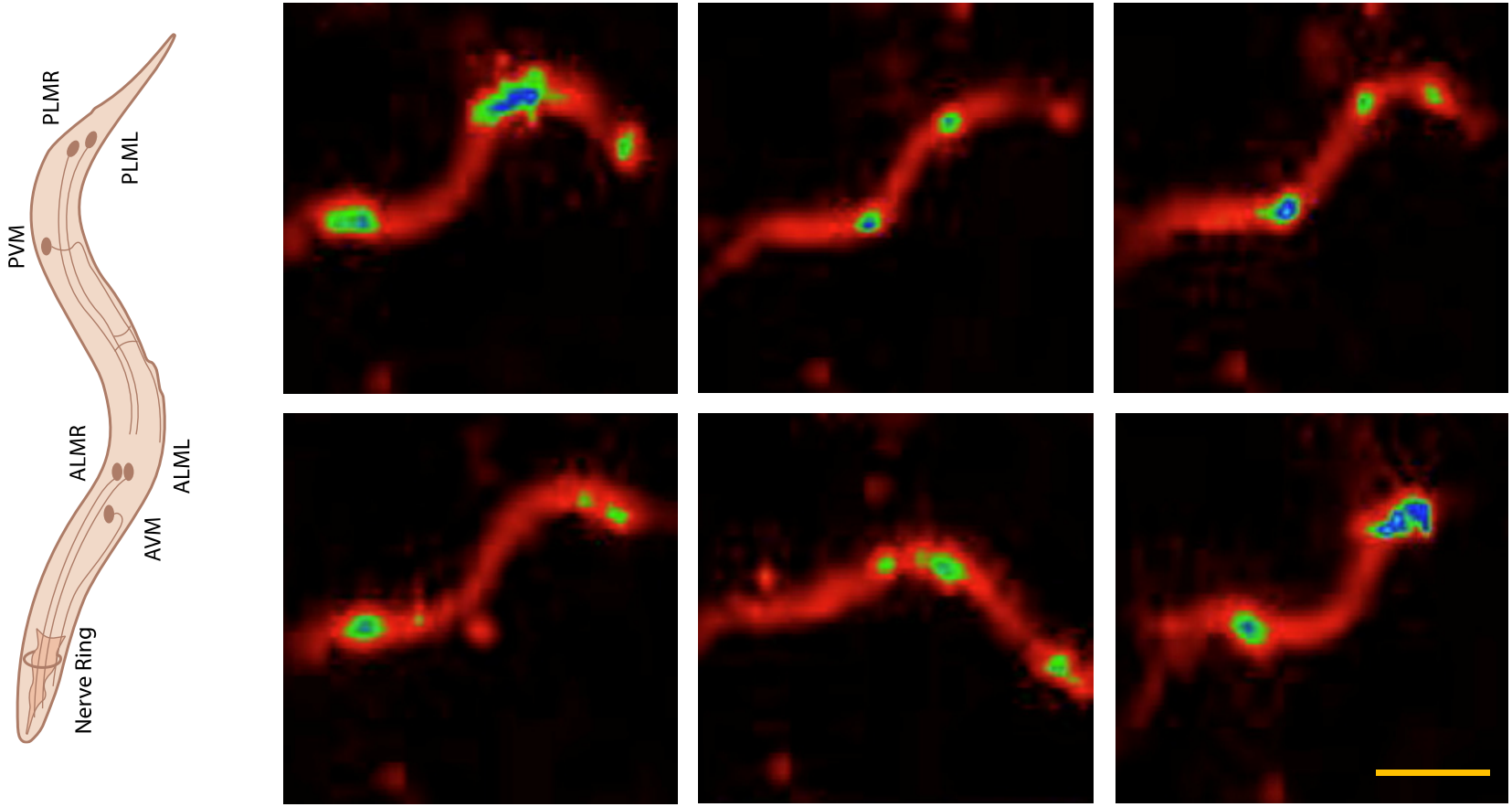

Figure 5: (a) Snapshots of the touch neurons activities in a single worm obtained using the bright probe. The worm takes different shapes as shown while performing frequent reversal movements causing graded activity in the mechanosensory touch neurons (PLM, PVM, ALM, AVM and the anterior nerve ring neurons). The scale bar corresponds to 500μm.

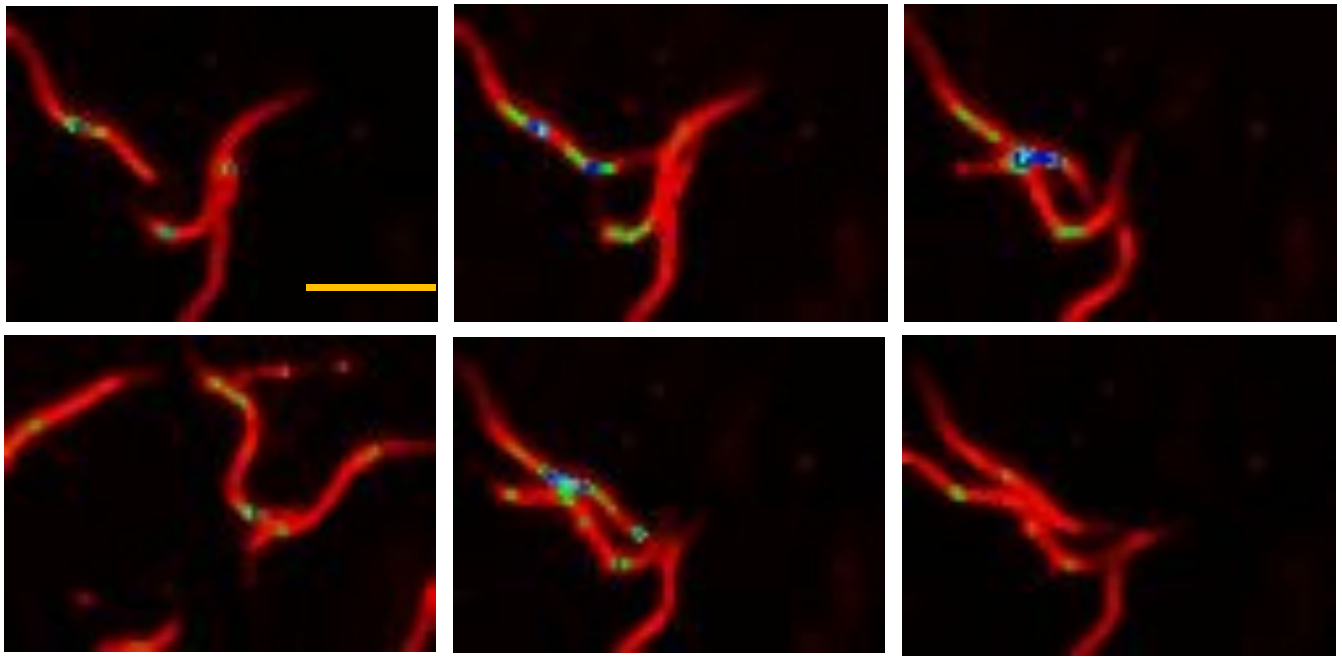

Figure 5: (b) Snapshots of activities of the touch neurons in a population of worms undergoing collision. Touch neurons respond to differential forces exerted on the colliding worms due to momentum transfer. The scale bar corresponds to 500μm.

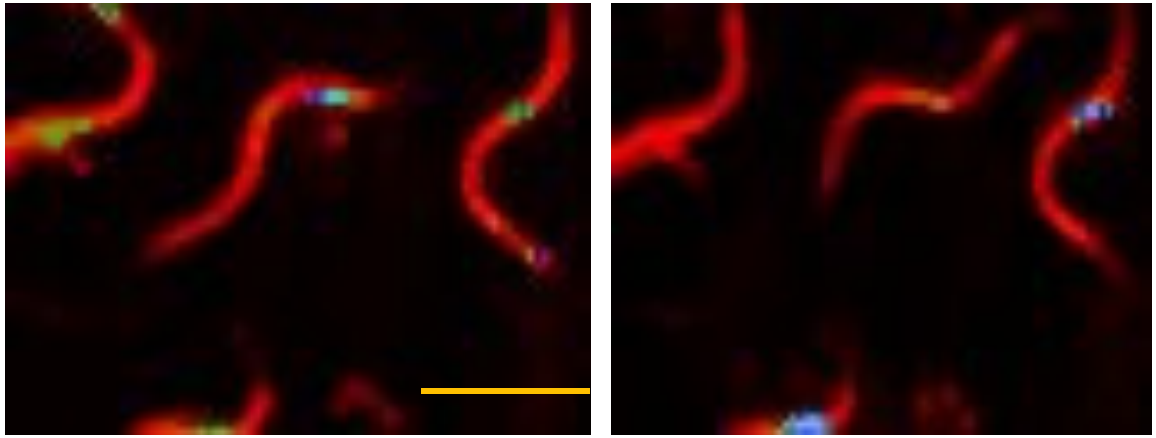

Figure 5c: Snapshots of varying levels of activity in touch neurons from a population of worms recorded in a single field of view. The scale bar corresponds to 500μm.

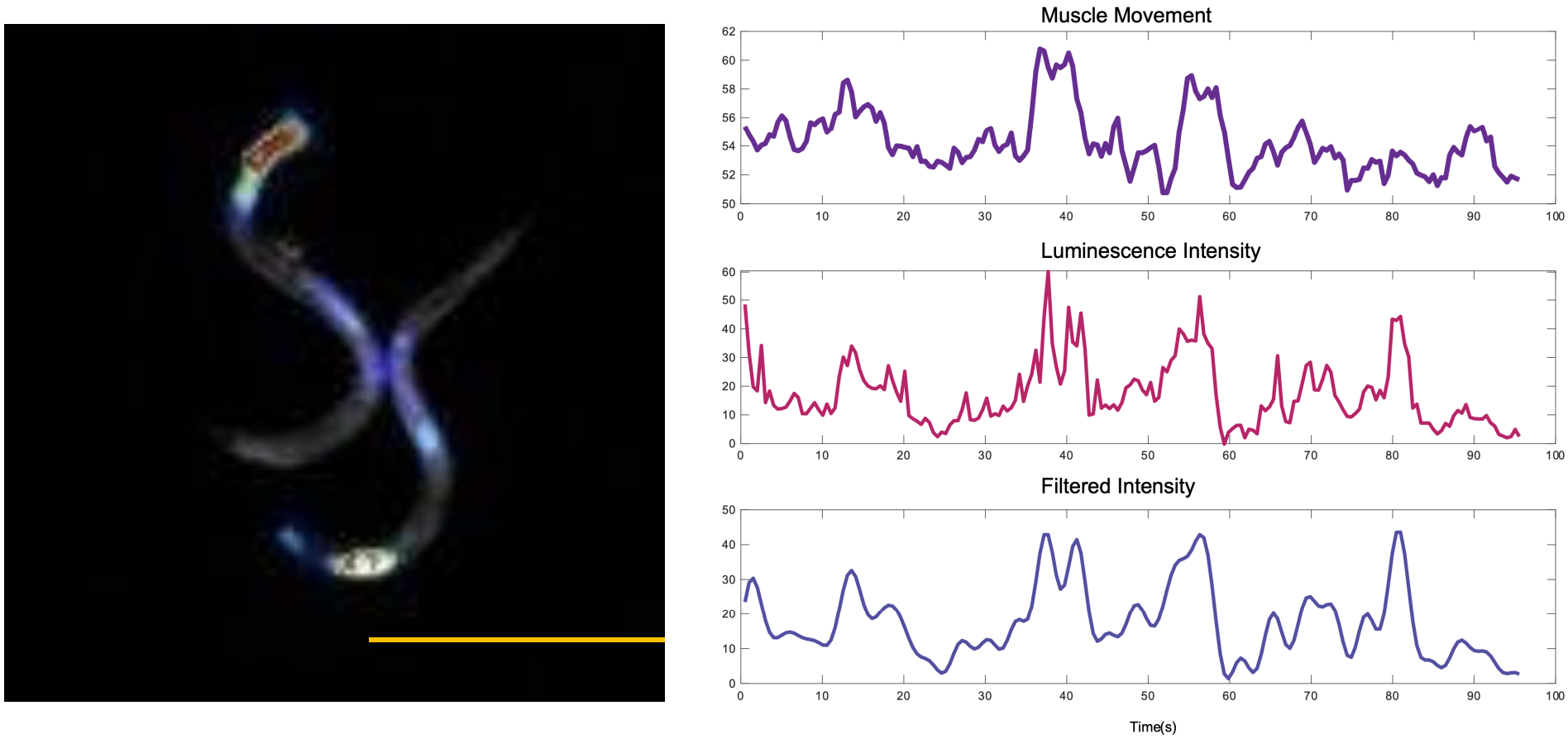

(a) (b)

Figure 6: (a) In vivo voltage imaging of C.elegans pharyngeal muscle activity. (b) Correlation between muscle movement and voltage recording using AMBER. The top panel shows a time trace of muscle movement from one of the animals. The middle panel shows the raw intensity trace recorded using AMBER, which correlates well with the muscle movement. The lower panel shows a filtered trace removing the high frequency features observed in the raw data. The data suggest the transfer function between voltage and muscle movement is a low pass filter. The scale bar corresponds to 500μm.